JOURNAL OF SPACECRAFT AND ROCKETS
Vol. 39, No. 2, March–April 2002

Six-Axis Vibration Isolation System Using Soft Actuators and Multiple Sensors

Doug Thayer,* Mark Campbell,† and Juris Vagners‡
University of Washington, Seattle, Washington 98195-2400
and
Andrew von Flotow§
Hood Technology Corporation, Hood River, Oregon 97031

Several types of Stewart platforms have been implemented by research groups to examine design and control issues in six-axis vibration isolation for space-based systems. Hood Technology Corporation and the University of Washington have taken the lessons learned from these various designs and developed a new hexapod that addresses the requirements of the Jet Propulsion Laboratory's planned spaceborne interferometry missions. This system is unique in its very soft axial stiffness (3-Hz corner frequency) for active isolation and pointing control, custom-designed voice coil actuator with a large displacement capability, and elastomeric flexures both for guiding the actuator and providing pivots at the end of each strut. In addition, there are four sensors in each strut for control topology design and evaluation. An overview of this unique six-axis isolator design and a summary of the control results for various sensor topologies, including multisensor and frequency-weighted isolation and pointing control, are presented. Controllers that experimentally achieved 20–25-dB reduction in vibration in all six degrees of freedom across the bandwidth of interest (5–20 Hz) are shown.

Nomenclature

A, B, C, D, Γ	=	input/output model matrices for hexapod
F_i	=	forces on the strut
G	=	linear quadratic regulator gain
$G(s)$	=	six-axis transmissibility
H	=	Kalman filter gain
I	=	transfer inertance
J	=	linear quadratic regulator cost functional
K_i	=	end flexure translational stiffness
K_L	=	lateral stiffness of strut
$K(s)$	=	multivariable controller
K_T	=	lateral dynamic stiffness of the strut
$K_{\theta i}$	=	end flexure rotational stiffness
L	=	strut length
$P(\omega)$	=	scalar measure of energy per unit frequency of the transmissibility
Q, R	=	state and input quadratic weights in J
u_i	=	translational displacement of strut
W, V	=	process and sensor noise intensities
$\boldsymbol{w}, \boldsymbol{v}$	=	vector of process and sensor noises
$\boldsymbol{x}, \boldsymbol{y}, \boldsymbol{u}$	=	state, input, and output vectors
ω	=	driving frequency

Introduction

THE cubic hexapod, or Stewart platform,[1] has become one of the most popular approaches for six-axis active vibration isolation in precision systems. The hexapod uses a minimum number of actuators for six-axis control and allows isolation to be targeted to a specific disturbance path on the structure. The cubic hexapod simplifies control topologies to allow decoupled controller designs that are identical for each strut. Furthermore, the configuration permits full six-axis positioning and pointing of the payload.

Several hexapods have been designed and constructed by researchers in the community. Each of these can be grouped into two different categories: hard active mount (HAM), where a stiff actuator, such as a piezoelectric, is used alone or in series with a soft spring and soft active mount (SAM), which uses a soft actuator, typically a voice coil, in parallel with a soft spring. Examples of HAM hexapods include designs by Intelligent Automation, Inc., Charles Stark Draper Laboratory, Inc., Harris, and CSA Engineering.[2–6] The use of soft actuators is demonstrated in hexapods built by Honeywell, Inc./Air Force Research Laboratory (AFRL) and the Jet Propulsion Laboratory (JPL) and the University of Wyoming.[7–9] Advantages of the SAM- over HAM-based systems include the following: 1) They have far more actuation stroke (1000 vs 50 μm), which allows for pointing control. 2) They have a soft corner frequency that allows a much lower frequency isolation. Disadvantages of the SAM-based systems include 1) the requirement that the payload mass be off-loaded during ground testing and 2) the requirement that the struts be bolted down before launch.

With few exceptions, the control strategy for six-axis hexapod systems has been classical.[3–9] The classical approach is used because the cubic hexapod decouples the dynamics into six individual strut systems that are approximately identical. This orthogonality allows the same control loop to be closed around each axis to create a decentralized multi-input/multi-output (MIMO) controller, which drastically simplifies the control because only a single-input/single-output (SISO) controller must be designed. In addition, this orthogonality is not restricted to the type or number of combinations of actuators and sensors on the local strut. This approach, however, is ultimately limited by the orthogonal assumption. For instance, when load cells are used for sensing, which is the case in many systems, lateral stiffness in the struts causes vibration paths that are not visible to the sensors.[9] These problems limit the achievable performance of the decentralized SISO approach.

Hood Technology Corporation (HT) and the University of Washington (UW) have designed and tested a unique hexapod design for spaceborne interferometry missions. By the use of lessons learned from these past approaches, several improvements in the hexapod design were implemented. This design, shown in Fig. 1, is similar to those built by JPL, which were also designed in

Received 13 December 2000; revision received 14 September 2001; accepted for publication 19 September 2001.

*Research Assistant, Department of Aeronautics and Astronautics. Member AIAA.
†Assistant Professor, Department of Aeronautics and Astronautics. Member AIAA.
‡Professor, Department of Aeronautics and Astronautics. Member AIAA.
§President. Member AIAA.

Table 1 Summary of current hexapods

Hexapod	Actuator	Actuation stroke, mm	Feedback sensors	Passive damping	Passive corner frequency	Off-load provision	Active bandwidth requirement, H_2
Intelligent automation	Magnetostrictive (HAM)	±0.127	Load cell, payload accelerometer	——	Rigid	Internal spring adjust	10–200
Draper	Piezoceramic (HAM)	±0.025	Load cell	——	Rigid	None	10–200
Harris/AIF	Piezoceramic (HAM)	±0.025	Base and payload accelerometers	——	Rigid	None	10–200
CSA UQP (SUITE)	Electromagnetic (HAM)	±0.020	Payload geophone	Elastomer ($\zeta \sim 0.05$)	15 Hz	None	3–100
Honeywell/ AFLR VISS	Voice coil (SAM)	±2	Payload accelerometer	Fluid ($\zeta \sim 0.2$)	1 Hz	External suspension	0.2–40
JPL	Voice coil (SAM)	±0.5	Load cell	Eddy current ($\zeta \sim 0.02$)	10–20 Hz	External suspension	1–100
HT/UW	Voice coil (SAM)	±5	Load cell, payload geophone, LVDT	Elastomer ($\zeta \sim 0.1$–0.2)	3 Hz	External suspension	0.3–30

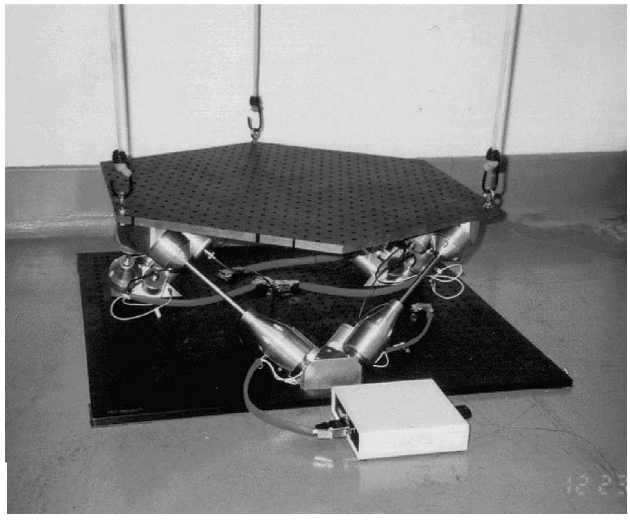

Fig. 1 HT/UW hexapod.

collaboration with one of the authors. The design presented here is a SAM system and extends the actuation stroke to 10,000 μm. This stroke is an order of magnitude increase in actuator displacement capability over other SAMs, giving this hexapod a much greater capability for pointing control. To improve isolation, the passive corner frequency of the system is 3 Hz, significantly lower than most other systems. Elastomer flexures and links, rather than steel, were also used to reduce lateral stiffness and improve passive performance at payload resonance and at microphonic frequencies (>100 Hz). The HT/UW system also includes a full array of sensors, including three-axis load cells, linear variable differential transformers (LVDTs) for differential position, and payload and base geophones. This sensor suite, the largest of its kind, allows the users to develop, test, and systematically compare many of the control topologies in a base system like never before. In addition, the soft elastomer flexures and three-axis load cells allow the evaluation of the lateral stiffness and orthogonality limitations of the hexapod.

This paper gives an overview of this unique six-axis isolator design and a summary of the control results for various sensor topologies, including multisensor and frequency-weighted isolation and pointing. The paper is organized as follows. First, an overview of current hexapod systems is given, followed by the detailed design of the HT/UW design. In this section, the uniqueness and research contributions of the HT/UW design are developed. This is followed by a summary of the control results, including single- and multiple-sensor decentralized active isolation, full multivariable active isolation, and combined active isolation and pointing.

Current Hexapod Research

Table 1 shows a summary of current hexapod experiments in the community that are focused on space systems. Intelligent Automation, Inc.,[2] has developed an HAM system. This hexapod uses a magnetorestrictive material known as Terfenol-D as a stiff actuator. Load cells and accelerometers are the feedback sensors and can be used alone or in combination in an adaptive control strategy. The struts are not designed for any passive isolation capability and use an internal spring to off-load the payload mass from the actuator. The system has an active vibration isolation bandwidth requirement of approximately 10–200 Hz.

Charles Stark Draper Laboratory[3] has a unique system because it is designed for a much larger payload than the other hexapods discussed here, namely, a 2.59-m-diam Cassegrain telescope. As with the Intelligent Automation, Inc., system, the control bandwidth requirement is 10–200 Hz, and no passive isolation capability is included. Each strut uses a piezoceramic for actuation with a load cell providing feedback in a classical controls approach. Accelerometers are added to allow multivariable control strategies to be implemented.

Another hexapod with piezoceramics was built by the Harris Corporation using their strut known as the active isolation fitting (AIF).[4] The unique aspect of their approach is the use of base and payload accelerometers for control. A classical loop is closed around each sensor, with the base accelerometer loop providing feedforward cancellation of incoming disturbances and the payload accelerometer loop inertially stabilizing the payload.

The final HAM system is the ultraquiet platform (UQP) constructed by CSA Engineering for the Space Test Research Vehicle-2 (Ref. 5). The newest version of this system from CSA is the Satellite Ultraquiet Isolation Technology Experiment (SUITE).[6] Stiff electromagnetic actuators provide the necessary control force with geophones used as vibration sensors. Again, the control strategy is classical, with a SISO loop closed around each strut. The UQP was designed with a passive corner frequency of approximately 15 Hz, which gives it a slightly lower control bandwidth requirement of 3–100 Hz.

The first of the SAM systems is a hexapod built by Honeywell, Inc., for AFRL, known as the Vibration Isolation and Suppression System (VISS).[7,8] In VISS, a voice coil is used as the soft actuator, and accelerometers are used for feedback. The corner frequency for the VISS is 1 Hz, which makes the control bandwidth requirement approximately 0.2–40 Hz. This very soft corner frequency means that the system has an external support system for off-loading the weight of the payload to prevent gravity sag. Also, because a voice coil is used as an actuator, the maximum possible displacement is more than an order of magnitude greater than that of any of the HAM systems. This large stroke gives VISS, as with most other SAM systems, significant capability for pointing control (<1 Hz).

JPL has designed and built several hexapod isolators, the most recent of which is a SAM system.[9] It is being developed primarily to improve the expected vibration environment on future spaceborne interferometers. JPL has constructed three nearly identical hexapods (the University of Wyoming hexapod differed only in that it had an internal spring for off-load). Tests on the JPL hexapod show the system to have a natural frequency of 10 and 20 Hz, and the target

control bandwidth is 1–100 Hz. As with VISS, the soft actuators are voice coils. The control strategy for this system has been classical, using load cells to provide feedback. The JPL system also includes both payload and base accelerometers, but to this point these have been used only to evaluate transmissibility performance and not for control. The HT/UW hexapod system most closely resembles the JPL systems.

HT/UW Hexapod

HT and UW have studied these systems to understand the benefits and drawbacks as applied to the spaceborne interferometry application. One of the authors (von Flotow) was also involved in the design of the JPL systems. As such, the HT/UW design addresses many of the issues with these systems, including the lateral stiffness, sensor topology, and control topology. This section details the unique characteristics of this system.

Flexures

A cubic six-axis hexapod attempts to decouple the six axes into six individual systems based on a single-axis strut element. One key assumption in this decoupling is that only axial forces are transmitted through each strut. This assumption is incorrect for several reasons. First, the rotational stiffness of the end flexures becomes important at low frequencies. At low frequencies, where the strut lateral transfer inertance (inertia) is less than strut lateral stiffness, the struts lateral effect can be seen in Fig. 2.

The lateral stiffness predicted by this model is

$$K_L = \left(K_{\theta_1} + K_{\theta_2}\right)/L^2 \tag{1}$$

This lateral stiffness leads to a performance limitation for active vibration isolation systems that use the struts axial force as a sensor, that is, a load cell. The strut transfer stiffness creates a low-frequency zero in the plant transfer function. This zero pair is usually sensitive and occasionally nonminimum phase, which creates stability and performance robustness issues. The nonminimum phase characteristics have been shown to be caused by a nonlinearity in the strut internal wiring.[10] Although there are compensation methods if the zeros are minimum phase, they usually involve plant inversion (high gain), which is not robust. For the JPL system, this zero appears within the active control bandwidth at approximately 2.6 Hz. In JPL's hexapod, the lateral stiffness is approximately 35 dB less than the struts axial stiffness (for a 20-Hz passive corner frequency).

The ideal hexapod has end flexures that are very soft rotationally and well damped, such that the zero pair is at a very low frequency and well damped, and the low-frequency gain is small. The HT/UW hexapod uses molded elastomer end flexures and achieves a lateral to axial stiffness ratio of greater than 40 dB.

At moderate frequencies, the isolator should be as soft and well damped as possible to work well passively and to allow the lowest isolation bandwidth. In the hexapod at these moderate frequencies, the strut lateral dynamics are that of a rigid body (inertia dominated rather than stiffness dominated). The lateral effect of the strut can be seen in Fig. 3. The lateral dynamic stiffness K_T predicted by this model is

$$K_T = \frac{(\omega^2 I)(K_1)(K_2)}{\omega^2 I + K_1 + K_2} \tag{2}$$

The HT/UW hexapod design minimizes the lateral stiffness using several approaches, including center of percussion mounting and

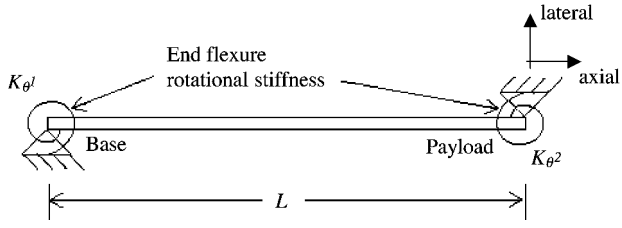

Fig. 2 Low-frequency model of the transverse disturbance transmission paths through a single strut.

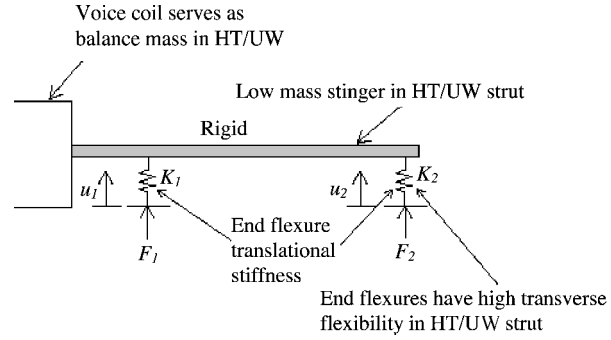

Fig. 3 Intermediate-/high-frequency model of the transverse disturbance transmission paths through a single strut.

low strut mass to minimize the transfer inertance and elastomer flexures with low lateral stiffness.

Center of Percussion Mounting

The payload end of the HT/UW strut has a flexure near its physical end (K_2), whereas there is a second flexure attached near its center of percussion (K_1). The center of percussion mounting is very close to the voice coil location. For modest frequencies, where the strut behaves as a rigid body, this drives the transfer inertance I toward zero. At higher frequencies, where the strut flexes laterally, this design innovation is probably less important.

Low Mass Strut

The HT/UW strut does not include the massive voice coil magnet. Rather, the magnet is hardmounted to the base, and the end flexures support only a lightweight stinger and voice coil. This reduces the transfer inertance I by approximately a factor of two.

End Flexures with Low Lateral Stiffness

Rather than use steel blade flexures with very high lateral stiffness, the HT/UW strut employs molded elastomeric flexures with low lateral stiffness K_1 and K_2. This limits the lateral dynamic stiffness of the strut to approximately

$$K_T \approx K_1 K_2/(K_1 + K_2) \tag{3}$$

The net effect of these design innovations is to reduce the lateral effect of each strut, both at low frequencies where feedback loop stability is at risk and at high frequencies where lateral disturbance transmission can otherwise exceed axial disturbance transmission.

Actuator

A custom-built voice coil actuator was designed for each strut to provide a maximum force of up to 10 lb, while dissipating as much as 56 W. The most interesting feature of these actuators is the very large maximum displacement (±5 mm) and large radial clearance (±1.5 mm). This gives the hexapod a great deal of capability for both low-frequency active isolation and precision pointing control. To take full advantage of this increased mechanical stroke, a low-noise linear amplifier was also designed.

Sensors

As outlined earlier, this platform contains a full array of sensors that provides the researcher with maximum flexibility in controller design by allowing almost any combination of sensors. The full sensor suite also allows an excellent testbed for an accurate and unbiased comparison of control topologies. The following sensors are on each of the six struts.

Three-Axis Load Cell

This is a custom 1-lb, three-axis force sensor developed by HT and Dytran Instruments, Inc. Although only the axial signal has traditionally been used for control, the other two transverse axes provide important information on other disturbance paths that are invisible to a one-axis load cell. The nominal sensitivity of the load cell is 17 mV/N.

LVDT

This sensor, which is built into strut, provides the differential position of the hexapod payload with respect to the base. This sensor

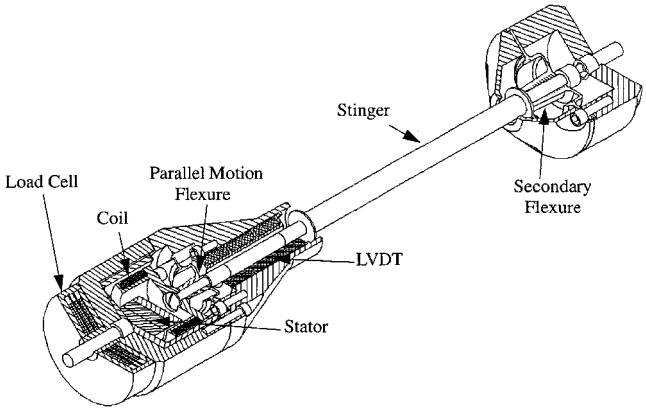

Fig. 4 Cutaway view of a single HT/UW strut. Note: Base and payload geophones mounted separately in parallel with strut.

can be used for open- and closed-loop positioning and pointing. The nominal sensitivity is 100 mV/mm with an accuracy of ±0.25%.

Geophones

Each of the six struts has a payload and base geophone for velocity information. This sensor is an excellent choice for vibration control because of its low-noise floor, better than that of a Q-3000 accelerometer in the frequency range of interest. The HT/UW hexapod uses the Geospace Corporation HS-1. It is small (247 g; 5.08 × 4.06 cm) and operates at a tilt angle up to 90 deg from vertical. The HS-1 geophone sensor has a corner frequency of 10 Hz and a sensitivity (±10%) of 0.453 V · cm · s.

Strut Integration

In integrating the innovative design characteristics of the strut with the voice coil actuator and suite of sensors, a housing was designed such that all of the design advantages are maintained while keeping it as simple as possible. Each of the six struts is identical. A diagram of the final HT/UW strut design is shown in Fig. 4. Note that the parallel motion flexure is the stiffness, denoted by K_1, and that it is attached near the center of percussion of the strut, that is, near the attachment of the voice coil. The secondary flexure is the stiffness K_2. The three-axis load cell is attached at the bottom of the strut.

The struts are built so that their corner frequency is a very soft 3 Hz but also adjustable over a wide range by exchanging different elastomer flexures. The passive damping in these elastomer links, specifically the parallel motion flexures, also enhances the performance of the system at low frequency and at the passive payload resonance. The damping is approximately 10%, much higher than the JPL system and most other soft and hard mount systems.

Electronics

Each strut is connected to its own electronics box that was designed to hold the amplifiers to drive the voice coil and the appropriate signal conditioning for each sensor output. One of these boxes is shown in the foreground of Fig. 1. Each strut requires an external 28 V dc and a maximum of 1.5 A to drive the voice coil and load cell. A ±7.5-V power rail is also used within each box for the sensor conditioning electronics using a switching regulator.

A final unique design feature of the HT/UW hexapod design is the power amplifier. The large stroke of each of the struts allows the hexapod to be used for active pointing control and disturbance suppression (from a cryocooler, for example), as well as active isolation. These control loops, however, require very different signal amplification. Active isolation usually requires very small sensor and actuator signals, whereas pointing and suppression usually require larger signals, depending on the system commands. A custom, low-noise power amplifier was designed to address this issue. The power amplifier is actually two different amplifiers: one with a low-current channel (0.5 A) used to drive the isolation loop and a second high-current channel (1.5 A) used drive the pointing and suppression loops. Both amplifiers are configured to provide current feedback, and their outputs are then summed at the voice coil.

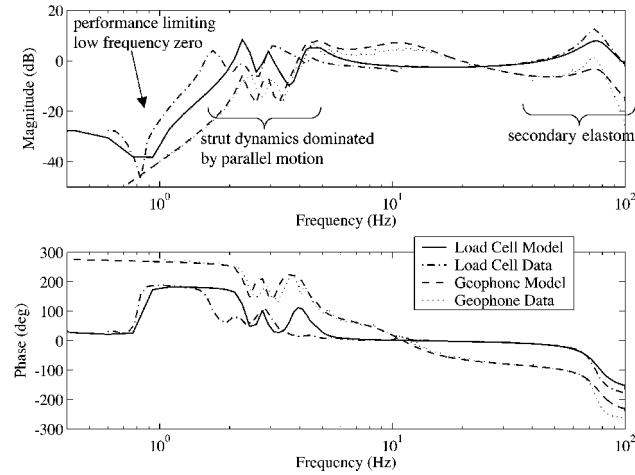

Fig. 5 Open-loop voice coil to geophone/load cell transfer functions for both the model and data.

Hexapod Integration

The 3-Hz corner frequency implies that the system requires the payload to be off-loaded. In this case, it is done externally by suspending the payload using three springs, as shown in Fig. 1. Each strut is attached at the top and bottom using an interface block. The faces of this block are cut at the proper angle so that the struts may be attached to form a cubic hexapod configuration. The geophone sensors are attached in parallel to the interface block. These blocks are then bolted to base and payload plates, which are cut from aluminum optical benches with $\frac{1}{4}$-in. holes spaced every inch. The current configuration of the system is shown in Fig. 1.

The final point about the HT/UW design is its flexibility with other configurations. The HT/UW hexapod was developed with the idea that it could be reconfigured into a shape other than a cubic hexapod in the future, if so desired. Historically, the cubic hexapod is used because all struts are orthogonal to adjacent struts, minimizing the effect of one strut on another. This allows the SISO control approach to be used. However, there may be other topologies where it may more beneficial to have the struts in another orientation. This would simply require a new set of interface blocks, which could be designed and constructed very quickly.

Model

Two models were developed for the hexapod. The first is a full six-axis model, including all cross-axial stiffnesses and damping, finite elements for each strut, as well as all sensors and actuators. The full model, which was used to analyze the final control designs and to design the multivariable controller, contains 70–100 states. The second model is a single-strut model because of the decoupling of the cubic hexapod into six similar axes. The single-axis model has eight states including sensor dynamics of the geophone and was used in the single-strut, decentralized control designs.

Figure 5 shows the full model and experimental open-loop transfer functions from the voice coil to the load cell and payload geophone for one strut on the integrated HT/UW hexapod. (Note that the single axis model is similar.) The load cell transfer function includes a low-frequency limiting gain of −25 dB, a low-frequency zero pair at 0.8 Hz, the soft-flexure-based dynamics near 3 Hz, and the stiffer secondary flexure dynamics near 75 Hz. The geophone dynamics are very small at low frequency due to the 10-Hz corner frequency, which acts as a high-pass filter. This corner also prevents good transfer function results below 0.5 Hz. The geophone transfer function also includes the soft-flexure-based dynamics near 3 Hz and the stiffer secondary flexure dynamics near 75 Hz. Note that the other strut transfer functions are similar.

Performance Metric: Six-Axis Transmissibility

Because of the problems created in evaluating the performance of a complex system like the hexapod, a unique performance metric, known as six-axis transmissibility, was developed by JPL.[9] The metric is determined by finding the 6 × 6 transfer function matrix

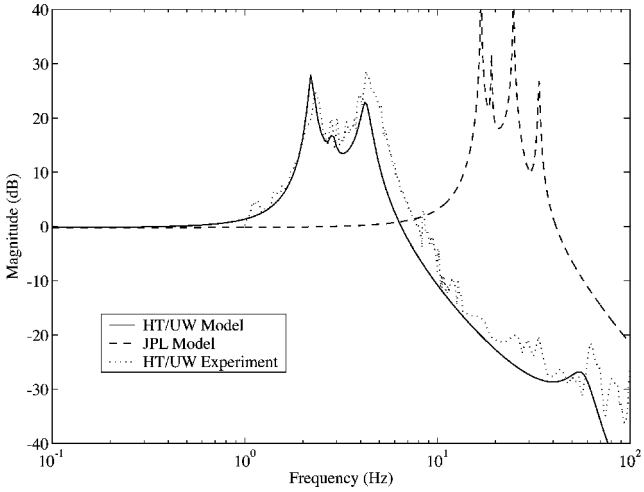

Fig. 6 Experimental and model-based six-axis transmissibility for the HT/UW and JPL hexapod systems.

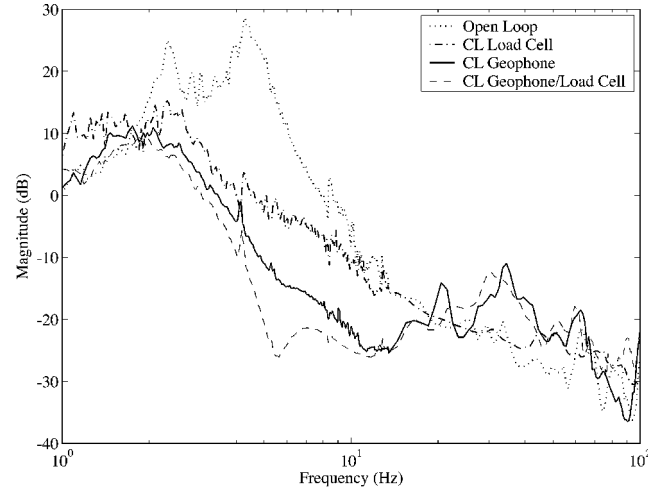

Fig. 7 Experimental closed-loop six-axis transmissibility results for the load cell (15.1 dB), geophone (22.4 dB), and combined geophone/load cell (23.7 dB) controllers.

from the six base acceleration inputs on each strut to the six payload accelerometer output $G(s)$. This matrix can then be evaluated over a desired frequency range using the Frobenius norm, resulting in a single frequency response that represents the effective transmissibility of a multiaxis isolator.

For this research, several modifications were made. First, base and payload velocity are used through the use of geophones, rather than of accelerometers, because of their improved performance on the HT/UW hexapod. Second, the two norm was used as the performance metric rather than the Frobenius norm because of its ties to signal analysis and probability concepts (such as 3σ values) and linear quadratic control. Based on the 6×6 transfer function matrix from the base to payload geophones, the two norm is given by

$$\|G\|_2^2 = \frac{1}{2\pi}\int_{-\infty}^{\infty} \mathrm{tr}[G(j\omega)G^*(j\omega)]\,\mathrm{d}\omega = \int_{-\infty}^{\infty} P(\omega)\,\mathrm{d}\omega \qquad (4)$$

where $P(\omega)$ is a scalar measure of the energy per unit frequency of the transmissibility. The area under this curve then gives the two norm.

Figure 6 compares the experimental six-axis transmissibility curve obtained from the actual data of the system to a 42-state model developed for the system. The full 48-state model contains six identical struts, each with models of the voice coil, stinger, flexures, sensor dynamics, and base and payload masses. The experimental data are produced by shaking the base plate (mounted on a foam pad) using large shaker. When the shaker is moved through each of the six degrees of freedom, it is possible to excite all of the dynamics of the system. The data from each degree of freedom are then added together ensure that all dynamic information for the system is captured.

Figure 6 shows that low-frequency signals pass through the hexapod, whereas a series of resonances occur at approximately 3 Hz. The transmissibility then rolls off at 40 dB per decade. In comparing the HT/UW and the JPL hexapods (also shown in Fig. 6), notice the large differences in the passive corner. The JPL system is much stiffer passively due to the use of steel flexures. The lower frequency and heavier damping of the HT/UW system is evident. There is another resonant frequency at 80 Hz due to the stiff secondary flexure in the system. Beyond this frequency, the experimental data show the influence of a payload plate bending. The experimental results match well up to approximately 80 Hz.

Controller Development and Experimental Results

A variety of control results have been developed and implemented on the HT/UW hexapod. Presented and discussed here are controllers based on decentralized single-strut, single-sensor controllers (SISO), decentralized controllers with two feedback sensors from each strut [single-input/multi-output (SIMO)], and full multivariable (MIMO) results. Also presented are the results from the combined active isolation and pointing controllers.

Decentralized, Single-Sensor Controllers

Two decentralized, single-sensor controller topologies were developed and tested: feedback of the load cell sensors to each local strut voice coil and feedback of the geophone sensor to the local strut voice coil. In each case, a decentralized MIMO controller was developed by integrating six identical SISO controllers. Single-strut controllers were designed using linear quadratic methods as well as classical methods, and the best results were similar for all methods. The classical controller is presented here because of its intuitive appeal.

A relatively simple third-order controller was designed using the geophones for feedback and demonstrated reasonable performance and good stability margins. The controller consists of a low-frequency second-order rolloff (corner of 0.2 Hz) to increase the loop gain near 3 Hz and two zeros at 10 Hz to counteract the geophone corner frequency. An additional pole at 25 Hz is used to roll off the system. Note that the SISO linear quadratic controller was very similar.

The experimental closed-loop six-axis transmissibility results are shown in Fig. 7. The controller actively softens the system corner frequency to approximately 1.5 Hz and reduces the rms of the transmissibility (from 0.8 to 30 Hz) by 22.4 dB. The model (not shown) predicts the softening to be to 0.6 Hz and a performance improvement of 20.4 dB. Because of a lower phase margin from computational delay and rolloff pole, a pop appears in the 35-Hz region of the geophone controller. Also, the mode at 60 Hz is a result of the ac power source in the electronics and not the system dynamics.

A load-cell-based controller was developed in a similar manner; a SISO single-strut controller was replicating for all six axes. Again both the classical and linear quadratic results are similar. The classical controller included a lag filter to provide sufficient phase margin at the lower crossover (1.2 Hz) and a high-pass filter to keep the excess gain below the crossover (1.2 Hz) below unity. This excess gain partly results from the low-frequency zero and partly from the low-frequency gain introduced by the lag filter. A low-pass filter was used to provide a rolloff before the resonance of the secondary flexure. Figure 7 shows the corresponding experimental closed-loop six-axis transmissibility results. The load cell controller, except in the 20–70 Hz range, did not perform as well as the geophone with respect to the rms metric (15.1 dB for the load cell controller vs 22.4 dB for the geophone controller).

The fundamental limitation of the load cell controller is the low-frequency zero pair. Any controller that uses the load cell sensor must use high gain near this region to boost the loop gain. This zero pair can be quite sensitive[10] such that a robust control methodology usually simply lowers the low-frequency gain. The affect of the low-frequency zero limitation is evident in the closed-loop transfer function, where the low-frequency passive mode (2 Hz) did not soften. The performance in this region is comparable to open loop.

In 1-g, because the cross-axial dependence (and this zero pair) is dominated by the payload suspension, a higher bay would result in a lower bounce suspension mode and, thus, reduce the zero frequency. On orbit, however, this zero would be significantly smaller, and the HT/UW hexapod would most likely allow control to well below 1 Hz using the load cell sensor.

Decentralized, Two Sensor Controllers

A decentralized single-strut, two-sensor controller was developed for the system, based again on the decentralized architecture. In this case, six identical SIMO controllers are integrated into a MIMO controller. The SIMO controller fed both the load cell and geophone sensors to the local voice coil in the strut. For the SIMO controllers, it was much simpler to move to a multivariable control scheme rather than classical.

Linear quadratic designs have been used for years by researchers for multivariable control.[11,12] The approach is relatively simple to use to develop a multivariable control law. Consider a state-space system:

$$\dot{\boldsymbol{x}} = A\boldsymbol{x} + B\boldsymbol{u} + \Gamma\boldsymbol{w}, \qquad \boldsymbol{y} = C\boldsymbol{x} + D\boldsymbol{u} + \boldsymbol{v} \tag{5}$$

The intensity of the process and sensor noise are defined as

$$E\lfloor \boldsymbol{w}(t+\tau)\boldsymbol{w}^T(t)\rfloor = W\delta(\tau), \qquad E\lfloor \boldsymbol{v}(t+\tau)\boldsymbol{v}^T(t)\rfloor = V\delta(\tau)$$

The linear quadratic cost function to be minimized is

$$J = \lim_{t\to\infty} E\left[\frac{1}{2}\int_0^\infty [\boldsymbol{x}(t)^T Q\boldsymbol{x}(t) + \boldsymbol{u}(t)^T R\boldsymbol{u}(t)]\,\mathrm{d}t\right] \tag{6}$$

where Q is a positive semidefinite state/performance weighting matrix and R is a positive definite control weighting. A state feedback gain matrix G and an analogous Kalman filter gain matrix H can then be found by solving the steady-state algebraic Riccati equation. In this case, the model-based controller takes the form

$$K(s) = G(sI - A + BG + HC)^{-1}H \tag{7}$$

One powerful tool in linear quadratic, active vibration isolation is the selection of the weighting matrices. As shown by Hyde,[13] the choice of Q, R, W, and V can be used to shape the system transmissibility. In this case, the Q/R ratio defines the low-frequency corner, and the W/V ratio defines the upper corner frequency. By the proper selection of these weighting matrices, it is possible to set the corner frequency of the active controller.

In addition to the SIMO sensor topology, a frequency weight was also added to the control design. The technique of frequency weighting was first proposed in Ref. 14. It is particularly well suited to the problem of vibration isolation because it allows the designer to shape the transmissibility curve while applying similar computational procedures. The only issue is that the size of the controller increases with the number of frequency weight states. For this work, a simple second-order filter is centered at 5 Hz to decrease more sharply the transmissibility in this region. It penalizes the performance in the bandwidth of interest, from 0.5 to 20 Hz.

The experimental six-axis transmissibility results for the decentralized SIMO closed-loop system are shown in Fig. 7. The controller bandwidth is approximately identical to the SISO geophone controller, but there are several key differences. First, the region of maximum attenuation due to active control has been moved from 15 Hz in the SISO geophone case back to 5 Hz. Note that the slope from 2 to 5 Hz is now −40 dB/decade, matching the rolloff of the frequency weight. In addition to the added performance, the 20–80 Hz region of control was more robust, with better phase margins at low and high frequency. The cost of this more capable controller is the increase in controller size from seven states to nine states for each of the six struts. The model predicts an rms isolation of 22.2 dB, whereas the data results indicate 23.7 dB.

Full Feedback Multivariable Controller

A full feedback multivariable controller (all six payload geophone sensors to all six strut actuators) was developed for the hexapod. The results, unfortunately, were quite poor. There were two primary reasons for this, each of which is based on the off-axis dynamics, that is, from one strut to another. First, the off-axis dynamics are very difficult to predict in the model, making them very difficult to control. However, the second, more important, reason is that the model contained many nonminimum phase zeros in the off-axis transfer functions, thus limiting the achievable control. Depending on the weightings used, the controller results varied between the load cell and geophone individual results shown in Fig. 7. In addition, by weighting the diagonal results much more, a decentralized controller similar to the earlier decentralized controllers was recovered.

Active Isolation and Pointing

One of the biggest benefits of the unique HT/UW design is the ability to do both multiaxis active isolation and pointing. This is an important new area that has only been addressed by the Honeywell, Inc./AFLR VISS experiment.[7,8] The feedback sensor used for pointing is the LVDT, mounted in parallel with the voice coil actuator. This sensor measures the elongation of each individual strut. The voice coil actuator is used both for pointing and isolation. One of the most important issues with combining active isolation and pointing is that the lower-frequency pointing loop usually requires much more actuator command (stroke, current). Therefore, to make the best use of the digital-to-analog converter (DAC) range (±5 V), the two control loops have separate DACs. The two control outputs (for pointing and isolation) are then adjusted with analog gains before they are added and sent to the voice coil actuator. Because the control frequency region for pointing is much lower than for isolation, it can be viewed as the dc component of the control signal. A simple schematic of the control architecture is shown in Fig. 8.

Two control loops were closed for isolation and pointing. The active isolation controller was identical to the decentralized two-sensor controller presented in the preceding section. The pointing controller was designed to minimize the interaction between the pointing and isolation control loops. A simple proportional–integral–derivative

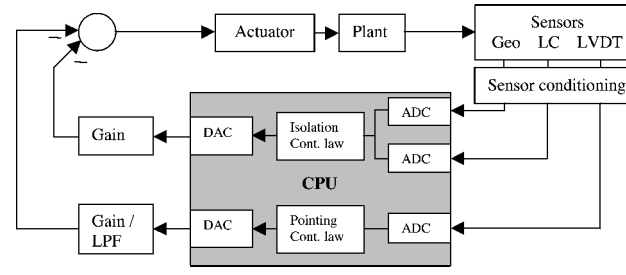

Fig. 8 Block diagram setup for the combined active isolation and pointing experiments.

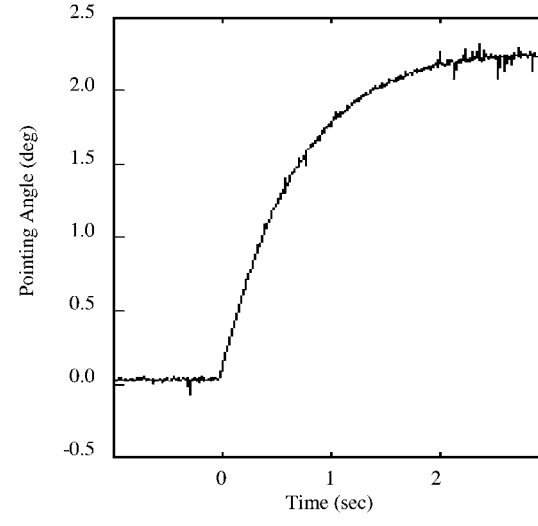

Fig. 9 Time history of the pointing controller response to a step function.

controller with a bandwidth of 1 Hz was used for servo pointing control. With both loops closed, a six-axis disturbance was applied to each of the base struts, and a reference step command was used to slew the hexapod top plate pointing angle 2.25 deg. The step response (pointing angle of the top plate of the hexapod) is shown in Fig. 9. The 2.25-deg slew was completed in approximately 3 s with little or no overshoot. The jagged response of the pointing angle was a result of 1) a small amount of jitter in the control loop and 2) output noise on the sensor. It is surmised that, with a better LVDT sensor, these results would improve. Overall, however, the combined isolation/pointing results using the HT/UW hexapod are promising.

Conclusions

HT and UW have designed and developed a hexapod that is unique when compared to other efforts in the area of active vibration control. A sensor suite with many of the most common vibration sensors (three-axis load cell, payload and base geophones, LVDT) allows objective comparison of different control approaches and architectures. In addition, the soft (2-Hz) heavily damped ($\zeta \sim 0.2$) passive dynamics (due to a low mass stinger/strut design with elastomer flexures) and the ± 5-mm stroke voice coil allow studies in combined isolation, large-angle pointing, and suppression to occur.

Experimental closed-loop control results using the hexapod have shown that controllers designed using a decentralized single-strut design work well when compared to full multivariable methodologies. Decentralized multivariable controllers were designed by replicating single-strut controllers for all six axes. Load-cell-only-based controllers performed the worst (15.1 dB), limited by the suspension springs and a pair of low-frequency zeros. Note, however, that the suspension springs will not be present in 0-g implementations. The geophone-only-based controllers performed much better at low frequency and achieved 22.4 dB. The combined geophone/load cell controller performed better than the single-sensor controllers (23.7 vs 15 and 22.4 dB). In addition, the geophone/load cell sensor controller was more robust than the load cell controller at low frequency (no inversion of lightly damped zeros) and more robust than the geophone controller at high frequency (larger phase margin). The full feedback multivariable design, not shown, did not add any benefit to the results because of the off-axis dynamics (mismodeling and nonminimum phase zeros). Initial combined active isolation and pointing results showed a simple 2.25-deg slew maneuver with no overshoot, results that are promising for the integrated isolation/pointing problem.

References

[1]Stewart, D., "A Platform with Six Degrees of Freedom," *Proceedings of the Institution of Mechanical Engineers*, Vol. 180, 1965–1966, pp. 371–386.

[2]Geng, Z., and Hayes, L., "Six Degree of Freedom Active Isolation Using the Stewart Platforms," *IEEE Transactions on Control Systems Technology*, Vol. 2, No. 1, 1994, pp. 45–53.

[3]Henderson, T., "Design and Testing of a Broadband Active Vibration Isolation System Using Stiff Actuators," *Proceedings of the 19th Annual AAS Guidance and Control Conference*, American Astronautical Society, San Diego, CA, 1996, pp. 481–500.

[4]Hyland, D., King, J., and Davis, L., "Active Vibration Isolation with Stiff Actuators and Inertial Sensors," *Actuator Technology and Applications: Proceedings of the Society of Photo-Optical Instrumentation Engineers (SPIE)*, Vol. 2865, Society of Photo-Optical Instrumentation Engineers (International Society for Optical Engineering), Bellingham, WA, 1996, pp. 93–102.

[5]Anderson, E., Leo, D., and Holcomb, M., "Active System for Vibration Isolation of Spacecraft Instruments," *Proceedings of the 19th Annual AAS Guidance and Control Conference*, American Astronautical Society, San Diego, CA, 1996, pp. 465–479.

[6]Anderson, E. H., Fumo, J. P., and Erwin, R. S., "Satellite Ultraquiet Isolation Technology Experiment (SUITE)," *IEEE Aerospace Conference*, IEEE Publications, Piscataway, NJ, 2000, pp. 299–313.

[7]Sullivan, J., Rahman, Z., Cobb, R., and Spanos, J., *Proceedings of the 1997 American Control Conference*, IEEE Publications, Piscataway, NJ, 1997, pp. 3974–3978.

[8]Foshage, J., Davis, T., Sullivan, J., Hoffman, T., and Das, A., "Hybrid Active/Passive Actuator for Spacecraft Vibration Isolation Suppression," *Actuator Technology and Applications: Proceedings of the Society of Photo-Optical Instrumentation Engineers (SPIE)*, Vol. 2865, Society of Photo-Optical Instrumentation Engineers (International Society for Optical Engineering), Bellingham, WA, 1996, pp. 104–122.

[9]Spanos, J., Rahman, Z., and Blackwood, G., "A Soft 6-Axis Active Vibration Isolator," *Proceedings of the 1995 American Control Conference*, IEEE Publications, Piscataway, NJ, 1995, pp. 412–416.

[10]Campbell, M., and Hauge, G., "Shaping the Transmissibility for Six-Axis Active Vibration Isolators," AIAA Paper 99-1287, Feb. 1999.

[11]Kwakernaak, H., and Sivan, R., *Linear Optimal Control Systems*, Wiley-Interscience, New York, 1972, pp. 311–321.

[12]Brogan, W., *Modern Control Theory*, 3rd ed., Prentice–Hall, Englewood Cliffs, NJ, 1991, pp. 651–666.

[13]Hyde, T., "Active Vibration Isolation for Precision Space Structures," Ph.D. Dissertation, Dept. of Aeronautics and Astronautics, Massachusetts Inst. of Technology, Cambridge, MA, Jan. 1996.

[14]Gupta, N., "Frequency Shaped Cost Functionals: Extension of Linear Quadratic Gaussian Design Methods," *Journal of Guidance and Control*, Vol. 3, No. 2, 1980, pp. 529–535.

R. B. Malla
Associate Editor